Combined analysis of the binary lens caustic-crossing event MACHO 98-SMC-1

Afonso, C; Alard, C; Albert, JN; Andersen, J; Ansari, R; Aubourg, E; Bareyre, P; Bauer, F; Beaulieu, J P; Bouquet, A

Published in:
Astrophysical Journal

DOI:
10.1086/308561

THE ASTROPHYSICAL JOURNAL, 532:340–352, 2000 March 20

COMBINED ANALYSIS OF THE BINARY LENS CAUSTIC-CROSSING EVENT MACHO 98-SMC-1

C. AFONSO,[1] C. ALARD,[2] J. N. ALBERT,[3] J. ANDERSEN,[4] R. ANSARI,[3] É. AUBOURG,[1] P. BAREYRE,[1,5] F. BAUER,[1] J. P. BEAULIEU,[6,7,8] A. BOUQUET,[5] S. CHAR,[9] X. CHARLOT,[1] F. COUCHOT,[3] C. COUTURES,[1] F. DERUE,[3] R. FERLET,[6] J. F. GLICENSTEIN,[1] B. GOLDMAN,[1,10,11] A. GOULD,[1,8,12] D. GRAFF,[1,12] M. GROS,[1] J. HAISSINSKI,[3] J. C. HAMILTON,[5] D. HARDIN,[1] J. DE KAT,[1] A. KIM,[5] T. LASSERRE,[1] É. LESQUOY,[1] C. LOUP,[6] C. MAGNEVILLE,[1] J. B. MARQUETTE,[6] É. MAURICE,[13] A. MILSZTAJN,[1] M. MONIEZ,[3] N. PALANQUE-DELABROUILLE,[1] O. PERDEREAU,[3] L. PRÉVOT,[13] N. REGNAULT,[3] J. RICH,[1] M. SPIRO,[1] A. VIDAL-MADJAR,[6] L. VIGROUX,[1] AND S. ZYLBERAJCH[1]

(The EROS Collaboration)

C. ALCOCK,[14,15] R. A. ALLSMAN,[16] D. ALVES,[14,17,18] T. S. AXELROD,[19] A. C. BECKER,[15,20,21] K. H. COOK,[14] A. J. DRAKE,[19] K. C. FREEMAN,[19] K. GRIEST,[15,23] L. J. KING,[15,22,24] M. J. LEHNER,[25] S. L. MARSHALL,[14] D. MINNITI,[14,26] B. A. PETERSON,[18] M. R. PRATT,[27] P. J. QUINN,[28] A. W. RODGERS,[19] P. B. STETSON,[29] C. W. STUBBS,[15,20] W. SUTHERLAND,[30] A. TOMANEY,[20] AND T. VANDEHEI[15,23]

(The MACHO/GMAN Collaboration)

S. H. RHIE,[22,31] D. P. BENNETT,[14,15,22,31] P. C. FRAGILE,[22] B. R. JOHNSON,[32] AND J. QUINN[22,31]

(The MPS Collaboration)

A. UDALSKI,[33] M. KUBIAK,[33] M. SZYMAŃSKI,[33] G. PIETRZYŃSKI,[33] P. WOŹNIAK,[34] AND K. ZEBRUŃ[33]

(The OGLE Collaboration)

AND

M. D. ALBROW,[35] J. A. R. CALDWELL,[36] D. L. DEPOY,[12] M. DOMINIK,[7] B. S. GAUDI,[12] J. GREENHILL,[37] K. HILL,[37] S. KANE,[18,38] R. MARTIN,[38] J. MENZIES,[35] R. M. NABER,[7] R. W. POGGE,[12] K. R. POLLARD,[35] P. D. SACKETT,[7] K. C. SAHU,[18] P. VERMAAK,[36] R. WATSON,[37] AND A. WILLIAMS[38]

(The PLANET Collaboration)

Received 1999 July 19; accepted 1999 November 8

[1] CEA, DSM, DAPNIA, Centre d'Études de Saclay, 91191 Gif-sur-Yvette Cedex, France.
[2] DASGAL, 77 avenue de l'Observatoire, 75014 Paris, France.
[3] Laboratoire de l'Accélérateur Linéaire, IN2P3 CNRS, Université Paris-Sud, 91405 Orsay Cedex, France.
[4] Astronomical Observatory, Copenhagen University, Juliane Maries Vej 30, 2100 Copenhagen, Denmark.
[5] Collège de France, Physique Corpusculaire et Cosmologie, IN2P3 CNRS, 11 pl. Marcellin Berthelot, 75231 Paris Cedex, France.
[6] Institut d'Astrophysique de Paris, INSU CNRS, 98bis Boulevard Arago, 75014 Paris, France.
[7] Kapteyn Astronomical Institute, Postbus 800, 9700 AV Groningen, The Netherlands.
[8] PLANET Collaboration member.
[9] Universidad de la Serena, Facultad de Ciencias, Departamento de Fisica, Casilla 554, La Serena, Chile.
[10] Departamento Astronomía, Universidad de Chile, Casilla 36-D, Santiago, Chile.
[11] European Southern Observatory, Casilla 19001, Santiago 19, Chile.
[12] Department of Astronomy, Ohio State University, Columbus, OH 43210.
[13] Observatoire de Marseille, 2 pl. Le Verrier, 13248 Marseille Cedex 04, France.
[14] Lawrence Livermore National Laboratory, Livermore, CA 94550.
[15] Center for Particle Astrophysics, University of California, Berkeley, CA 94720.
[16] Supercomputing Facility, Australian National University, Canberra, ACT 0200, Australia.
[17] Department of Physics, University of California, Davis, CA 95616.
[18] Space Telescope Science Institute, 3700 San Martin Drive, Baltimore, MD 21218.
[19] Mt. Stromlo and Siding Spring Observatories, Australian National University, Weston, ACT 2611, Australia.
[20] Departments of Astronomy and Physics, University of Washington, Seattle, WA 98195.
[21] MPS Collaboration member.
[22] Department of Physics, University of Notre Dame, Notre Dame, IN 46556.
[23] Department of Physics, University of California, San Diego, CA 92093.
[24] Max-Planck-Institut für Astrophysik, Karl-Schwarzschild-Strasse 1, Postfach 1523, D-85740 Garching, Germany.
[25] Department of Physics, University of Sheffield, Sheffield S3 7RH, England, UK.
[26] Departmento de Astronomia, P. Universidad Católica, Casilla 104, Santiago 22, Chile.
[27] Center for Space Research, MIT, Cambridge, MA 02139.
[28] European Southern Observatory, Karl-Schwarzschild-Strasse 2, D-857 48, Garching, Germany.
[29] National Research Council, 5071 West Saanich Road, RR 5, Victoria, BC V8X 4M6, Canada.
[30] Department of Physics, University of Oxford, Oxford OX1 3RH, England, UK.
[31] MACHO/GMAN Collaboration member.
[32] Tate Laboratory of Physics, University of Minnesota, Minneapolis, MN 55455.
[33] Warsaw University Observatory, Al. Ujazdowskie 4, 00-478 Warszawa, Poland.
[34] Princeton University Observatory, Princeton, NJ 08544-1001.
[35] University of Canterbury, Department of Physics and Astronomy, Private Bag 4800, Christchurch, New Zealand.
[36] South African Astronomical Observatory, P.O. Box 9, Observatory 7935, South Africa.
[37] University of Tasmania, Physics Department, G.P.O. 252C, Hobart, Tasmania 7001, Australia.
[38] Perth Observatory, Walnut Road, Bickley, Perth 6076, Australia.

ABSTRACT

We fit the data for the binary lens microlensing event MACHO 98-SMC-1 from five different microlensing collaborations and find two distinct solutions characterized by binary separation d and mass ratio q: $(d, q) = (0.54, 0.50)$ and $(d, q) = (3.65, 0.36)$, where d is in units of the Einstein radius. However, the relative proper motion of the lens is very similar in the two solutions, 1.30 km s^{-1} kpc^{-1} and 1.48 km s^{-1} kpc^{-1}, thus confirming that the lens is in the Small Magellanic Cloud. The close binary can be either rotating or approximately static but the wide binary must be rotating at close to its maximum allowed rate to be consistent with all the data. We measure limb-darkening coefficients for five bands ranging from I to V. As expected, these progressively decrease with rising wavelength. This is the first measurement of limb darkening for a metal-poor A star.

Subject headings: astrometry — dark matter — gravitational lensing — Magellanic Clouds

1. INTRODUCTION

The binary lens microlensing event MACHO 98-SMC-1, found by the MACHO collaboration (Alcock et al. 1999a) in observations toward the Small Magellanic Cloud (SMC), was observed by five different groups. Each group attempted to measure or constrain the relative lens source proper motion by fitting the observed light curve to a binary lens model, and each concluded that the proper motion is consistent with the lens being in the SMC rather than the Galactic halo (Afonso et al. 1998 [EROS]; Albrow et al. 1999a [PLANET]; Alcock et al. 1999a [MACHO/GMAN]; Udalski et al. 1998b [OGLE]; Rhie et al. 1999 [MPS]). Despite this unanimous opinion, there are several reasons for taking a closer look at this event.

First, Albrow et al. (1999c) have subsequently developed a more robust method for finding binary lens solutions that are consistent with a given light-curve data set. They found a broad set of degeneracies for the fit to MACHO 98-SMC-1 based on PLANET data and showed that based on these data alone the proper motion could not be constrained to better than a factor of 4. Such degeneracies are likely to be endemic to binary lens fitting (Dominik 1999a). Albrow et al. (1999c) showed that by including additional data it would be possible to remove at least some of these degeneracies, but they argued that one major ambiguity (between "wide" and "close" binaries) might be difficult to resolve. Hence, it is important to determine whether these degeneracies can in fact be resolved by combining all available data. In particular, the OGLE and MPS data together constrain the first caustic crossing, the MACHO data constrain the baseline, the PLANET data give excellent coverage of the main part of the second caustic crossing, and the EROS data give similar coverage of the end of the second caustic crossing.

Second, caustic-crossing binary events allow one, in principle, to measure the limb-darkening profile of the source star, as Albrow et al. (1999b) have done for a K giant using MACHO 97-BLG-28. The source in MACHO 98-SMC-1 is an A star as determined from both its colors (Albrow et al. 1999a; Rhie et al. 1999) and its spectrum (Albrow et al. 1999a). Since it is in the SMC, it is almost certainly metal-poor. If the limb darkening were measured, it would be the first such measurement for a metal-poor A star. The caustic crossing occurred while the source was visible from South Africa. The PLANET South African Astronomical Observatory (SAAO) data have excellent coverage of the main part of the caustic crossing, and it therefore might be possible to measure the limb darkening from these data alone using a variant of the method of Albrow et al. (1999c) which is described more fully in § 3. However, it is not clear to what degree the degeneracies in the overall fit would compromise such a determination. By fitting all the data these degeneracies could be partially or totally removed. The EROS data from Chile provide excellent coverage of the end of the crossing, and the MACHO/GMAN data also cover the end of the crossing. Neither of these data sets can determine the limb darkening without fixing the characteristics of the caustic crossing, which in turn requires the PLANET data.

Third, the light-curve coverage of MACHO 98-SMC-1 is one of the best of any binary lens event yet observed. It is therefore an excellent laboratory in which to search for additional, unanticipated anomalies that may be present in microlensing events but have not yet been noticed.

The implications of the proper-motion measurement for MACHO 98-SMC-1 for the nature of the lenses have been debated by several authors. Di Stefano (1999) has argued that most lenses detected along all lines of sight are normal stellar binaries and that MACHO 98-SMC-1 tends to support the view that the lenses seen toward the Magellanic Clouds are in the Clouds themselves. By contrast, Honma (1999) has argued that the halo proper-motion distribution could plausibly extend as low as the upper end ($\sim$2 km s^{-1} kpc^{-1}) of the range of estimates for the proper motion of MACHO 98-SMC-1 and moreover, that there is a significant bias toward detecting binary lenses with lower than average proper motions. He therefore concluded that MACHO 98-SMC-1 could well be a halo lens. Kerins & Evans (1999) developed a mathematical framework within which models of the lens distribution could be tested against a relative handful of determinations of lens locations. In applying their technique, they counted MACHO 98-SMC-1 as securely in the SMC. However, they showed that the discriminatory power of this determination depended critically on whether one assumed that the SMC halo is populated by similar objects as the Galactic halo. If the SMC and Milky Way halos are populated by similar objects, no firm conclusion could be drawn from a single detection; otherwise the proper-motion measurement favors stars in the SMC as the source of lenses.

In § 2 we briefly review the data that are available for this event. In § 3 we summarize and extend the Albrow et al. (1999c) method for finding binary lens solutions. In § 4 we present our results for static binaries, including measurement of the limb-darkening coefficients. In § 5 we derive the proper motion which in turn determines the projected separation of the binary. We use the latter quantity to constrain the period of binary orbit. We consider rotating binary models that satisfy this constraint in § 6. Finally, in § 7 we study the relationship of the solutions derived here to those reported in earlier investigations that were based on subsets of our combined data set. We show that all the close-binary solutions are in fact different positions within one broad minimum in χ^2. The wide-binary solutions of Albrow (1999c) represent another broad minimum. We also resolve some puzzling discrepancies between different solutions.

2. DATA

We describe all dates using HJD′ = HJD − 2,450,000.0, where HJD is the Heliocentric Julian Date. The reported times are the midpoints of the exposures. We combine a total of 14 light curves obtained at eight different telescopes. These were reduced using various photometry packages as described below. In all cases, points that failed internal tests of these packages were eliminated prior to beginning the fitting process.

The first two light curves were taken in the (broad nonstandard) MACHO *R* and MACHO *B* filters on the 1.3 m telescope at the Mount Stromlo and Siding Spring Observatory (MSSSO) near Canberra, Australia. These contain 727 and 735 points, respectively, beginning about 5 years before the event and ending 81 days after the second caustic crossing at HJD′ ∼ 982.6. The Mount Stromlo 1.3 m telescope is normally used to search for microlensing events and hence typically takes one exposure per clear night. However, because of the importance of this event, a total of 23 exposures were obtained during the nights just before and after the second caustic crossing. The next two curves were taken in the (standard Johnson/Cousins) *R* and *B* filters on the 0.9 m telescope at the Cerro Tololo Inter-American Observatory (CTIO) near La Serena, Chile. These contain 83 and 22 points, respectively, beginning 7 days before the first caustic crossing at HJD′ ∼ 970.5 and ending 6 days after the second crossing. MACHO has 1 hr per night on this telescope, which was mostly dedicated to MACHO 98-SMC-1 during this period of observation. All four of these light curves were reported by Alcock et al. (1999a). However, all the points after the first caustic crossing of the MSSSO data were rereduced using image subtraction[39] (Tomaney & Crotts 1996) which we determined has somewhat smaller errors than the original SoDoPHOT reductions. These include, respectively, 16 and 21 late-time points (more than 24 days after the second caustic crossing) that were not previously reported by Alcock et al. (1999a).

Next is the OGLE (standard Cousins) *I*-band curve from the 1.3 m Warsaw telescope at Las Campanas, Chile. The images are from OGLE's routine monitoring of the SMC to search for microlensing events, and OGLE made no special effort to observe this event. Rather, they analyzed their images after the event was over and found seven measurements during the interval from 4 days before the first caustic crossing to 4 days after the second. As discussed by Udalski et al. (1998b), the primary interest in this relatively small data set comes from the second data point on HJD′ = 970.9037, which is highly magnified ($A \sim 29$) and therefore comes either just before or just after the first caustic crossing.

The sixth and seventh curves were taken in (broad nonstandard) EROS *R* and EROS *B* filters on the 1.0 m Marly telescope at the European Southern Observatory at La Silla, Chile. Normally, this telescope is operated in survey mode to search for microlensing events. However, it was down for maintenance during most of the time that MACHO 98-SMC-1 was inside the caustic and recommenced operations only on the night of the second caustic crossing. In light of the importance of MACHO 98-SMC-1, the telescope was entirely dedicated to observing this event during this night and made several observations per night for the next 15 nights, whereupon it resumed normal operations. The observations of the first night were previously reported by Afonso et al. (1998). The rest of the observations are reported here for the first time. All the observations have been rereduced using an improved version (Alard 1999) of the algorithm used by Afonso et al. (1998). There were a total of 111 observations in *R* and 131 in *B*. These include about eight points in each band from 2 years before the event and about another eight from the year after the event when the source is approaching baseline.

The eighth curve is based on the (standard Cousins) *R*-band observations taken by the MPS collaboration using the 1.9 m telescope at MSSSO. A total of 34 observations were taken from just before the first caustic crossing until 4 days after the second. In addition, there is one late-time baseline measurement taken 67 days after the caustic crossing. These observations were earlier reported by Rhie et al. (1999). Of particular note is the first observation on HJD′ = 970.0485, which is clearly before the caustic crossing. This data point, combined with the OGLE data point 0.9 days later, strongly constrains the time of the first crossing.

The ninth through 13th curves are based on standard Cousins *I*-band observations taken by the PLANET collaboration using the SAAO 1 m telescope at Sutherland, South Africa, the Yale-CTIO 1 m telescope, the CTIO 0.9 m telescope, and the Canopus 1 m telescope near Hobart, Tasmania. The SAAO data are divided into two groups because of a change in the CCD detector at HJD′ = 980.0, 2 days before the caustic crossing. The five PLANET data sets comprise, respectively, 13, 175, 32, 13, and 1 observations. The CTIO 0.9 m telescope data cover only the interior of the caustic, beginning 3 days after the first crossing and ending 4 days before the start of the second. The Canopus data contain only one point about 1 day before the second crossing. The Yale-CTIO 1 m telescope data begin 4 days before the second crossing and end 14 days after it. The SAAO 1 m telescope data begin 5 days after the first caustic and end 44 days after the second. Of all the observations, only the SAAO data cover the peak of the second caustic crossing. Moreover, they do so quite densely. Most of these data were previously reported by Albrow et al. (1999a, 1999c). However, all of the SAAO data after HJD′ = 980.0 have been rereduced using image subtraction (Alard 1999) which we found produces significantly lower errors and fails significantly less frequently than even the best DoPhot reductions previously reported by Albrow et al. (1999c). Details of this comparison will be given elsewhere. In addition, we have eliminated the SAAO data from the first night, HJD′ = 975, because there was yet another CCD change on HJD′ = 976.0 rendering the conditions on this night unique.

Finally, the 14th light curve is based on standard Johnson *V*-band observations taken by the PLANET collaboration using the SAAO 1 m telescope. These comprise 24 observations including 14 taken during the second caustic crossing and 10 taken over the next 32 days. These data were used by Albrow et al. (1999a) to determine the *V*

[39] See also http://www.astro.washington.edu/austin/dip/software.html.

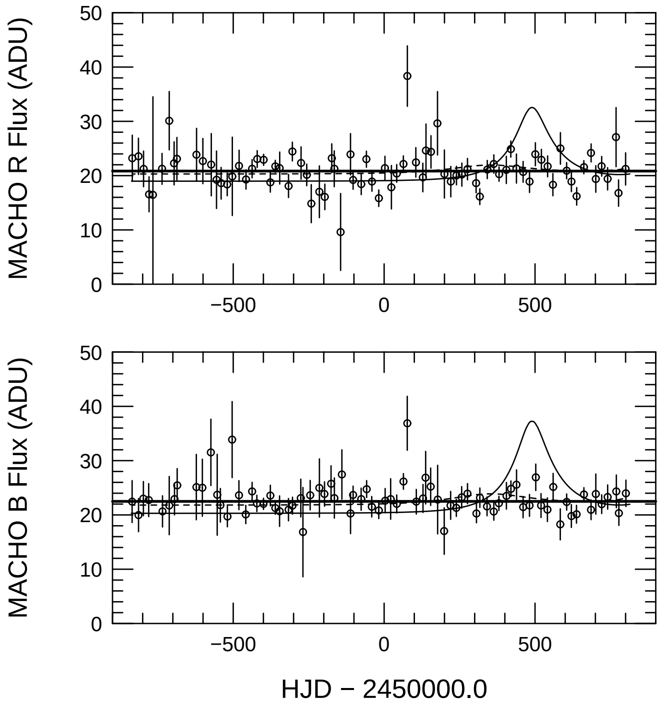

FIG. 1.—MACHO B and R data for MACHO 98-SMC-1 binned in 20 day intervals for the period before HJD′ = 810. The bold lines are the values for the baseline flux from the close-binary solution, $(d, q) = (0.54, 0.50)$. The event shows no significant deviation from baseline during this early period. The solid lines are from the best fit for the *nonrotating* wide binary $(d, q) = (3.25, 0.24)$, which is clearly ruled out by the data. However, a wide binary with a 75 yr period and a nearby $(d, q) = (3.65, 0.36)$ is permitted. Its early light curve is shown as a dashed curve that is barely distinguishable from a flat baseline curve.

brightness of the source and also its $V-I$ color, but have not previously been made available.

In a preliminary fit to the data, we find that four data points are significant outliers. These are the SAAO point at HJD′ = 979.6424, the MACHO B point at HJD′ = 982.2061, the EROS R point at HJD′ = 982.8427, and the MACHO B point at HJD′ = 997.1607, with residuals of −5.4, −4.9, −4.1, and 3.9 σ, respectively. We eliminate these from future modeling. We renormalize the quoted errors from each light curve by a factor so as to force χ^2/dof (degree of freedom) to be unity for that curve. The factors are MACHO R (SoDoPHOT): 1.12; MACHO B (SoDoPHOT): 1.12; MACHO R (image subtraction): 1.26; MACHO B (image subtraction): 1.58; MACHO-CTIO R: 0.94; MACHO-CTIO B: 1.10; OGLE I: 1.00; EROS R: 1.32; EROS B: 0.96; MPS R: 1.80; PLANET-SAAO (HJD′ < 980) I: 1.04; PLANET-SAAO (HJD′ > 980) I: 0.97; PLANET-Yale-CTIO I: 0.97; PLANET-CTIO I: 0.90; and PLANET-SAAO V: 2.21. The PLANET-Canopus I was not renormalized because there is only one point. The precise value of the renormalization factors depends slightly on which solution is adopted, but we find that our results are not sensitive to these small changes. We bin the early MACHO R and B data in 20 day intervals (see Fig. 1). With this binning, there are a total of 1018 data points.

3. METHOD

To analyze these data, we follow and slightly extend the method of Albrow et al. (1999c). We first review this method and its motivation and then discuss its extension.

Events where a nonrotating binary lens passes in front of a uniform finite source are described by $7 + 2n$ parameters, where n is the number of observatories: three parameters correspond to the three geometrical parameters of a point-like single lens (Einstein timescale $t_{\rm E}$, impact parameter u_0, and time of closest approach t_0); three other parameters characterize its binary nature (mass ratio q, separation d in units of the Einstein radius, and angle α of the source trajectory relative to the binary axis); one, ρ_*, describes the size of the source relative to the Einstein ring; and there are n parameters for the source flux, $F_{s,1}, \ldots, F_{s,n}$, and n for the unlensed background light, $F_{b,1}, \ldots, F_{b,n}$, that is, one pair for each of the n observatories. For events where the source crosses a fold caustic, one may define several additional useful parameters which can be derived from these $7 + 2n$, including the position within the Einstein ring where the source center crosses the caustic, $\boldsymbol{u}_{\rm cc}$, the time of the caustic crossing, $t_{\rm cc}$, the angle ϕ of the source trajectory relative to caustic at the crossing, the half-duration of the crossing Δt, and the radius crossing time $t_* \equiv \Delta t \sin \phi$. Generally, it is not difficult to find a set of parameters that yield a satisfactory fit to the data. However, it is often unclear whether there exist other equally good or better fits. One would like to make a systematic search through parameter space, but because of the size and complexity of the parameter space, a brute-force search is out of the question.

Albrow et al. (1999c) showed that for events with a well-observed caustic crossing, it is possible to greatly reduce the space of allowed solutions, thereby permitting a systematic search of the remaining parameter space. The method proceeds in three steps. First, the caustic crossing is fit to a five-parameter function. Second, these parameters are used to constrain a coarse-grained but systematic search through parameter space for solutions that can accommodate the non–caustic-crossing data. Third, final solution(s) are found by χ^2 minimization using the results from the coarse-grained search as initial guesses.

In the first step, the light curve is fit to a five-parameter curve of the form

$$F(t) = \left(\frac{Q}{\Delta t}\right)^{1/2} G_0\left(\frac{t - t_{\rm cc}}{\Delta t}\right) + F_{\rm cc} + \tilde{\omega}(t - t_{\rm cc}) \,, \tag{1}$$

where

$$G_0(\eta) \equiv \frac{2}{\pi} \int_{\max(\eta,\,-1)}^{1} dx \left(\frac{1 - x^2}{x - \eta}\right)^{1/2} \Theta(1 - \eta) \tag{2}$$

is the normalized light curve of a (second) caustic crossing with a uniform source and Θ is a step function. Here Q is related to the rise time of the caustic (defined more precisely below), $F_{\rm cc}$ is the magnified flux from the source when it is immediately outside the caustic, and $\tilde{\omega}$ is the slope of the light curve immediately outside the caustic. Using the PLANET data, Albrow et al. (1999c) found

$$Q = (15.73 \pm 0.35) F_{20}^2 \text{ days} \,,$$
$$t_{\rm cc} = (982.62439 \pm 0.00087) \text{ days} \,,$$
$$\Delta t = (0.1760 \pm 0.0015) \text{ days} \,, \tag{3}$$

$$F_{\rm cc} = (1.378 \pm 0.096) F_{20} \,,$$
$$\tilde{\omega} = (0.02 \pm 0.10) F_{20} \text{ days}^{-1} \,, \tag{4}$$

where F_{20} is the flux from an $I = 20$ star. For the first step, we simply adopt the results summarized in equations (3) and (4).

In the second step, the search of the full parameter space is substantially narrowed by making use of these caustic-crossing parameters with the following relations between observed and theoretical quantities:

$$F_{\rm cc} = A_{\rm cc} F_s + F_b \; , \quad F_{\rm base} = F_s + F_b \; , \tag{5}$$

$$t_r = u_r t_{\rm E} |\csc \phi| \; , \quad Q = F_s^2 t_r \; , \tag{6}$$

$$\Delta t = t_{\rm E} \rho_* |\csc \phi| \; . \tag{7}$$

Here F_s is the source flux, F_b is the background flux, $F_{\rm base}$ is the baseline flux, $A_{\rm cc}$ is the total magnification of the three nondivergent images at the position of the caustic, and u_r characterizes the square root singularity of the caustic. That is, in the neighborhood of the singularity, the total magnification of the two divergent images is given by $A_{\rm div}(u) = (\Delta u_\perp / u_r)^{-1/2}$, where $\Delta u_\perp$ is the perpendicular distance from the position u to the caustic in units of the Einstein radius, $\theta_{\rm E}$. The Einstein crossing time is $t_{\rm E} = \theta_{\rm E}/\mu$, where μ is the relative source lens proper motion, $\theta_{\rm E}^2 = (4GM/c^2)(D_{LS}/D_L D_S)$, M is the total mass of the binary, D_L and D_S are the distances to the lens and source, and $D_{LS} \equiv D_S - D_L$. Finally, t_r is a parameter that characterizes the rise time of the caustic.

In an ideal world, $t_{\rm cc}$, Q, $F_{\rm cc}$, and $F_{\rm base}$ would be measured exactly. In this case, the search could be reduced to four parameters (d, q, l, $t_{\rm E}$). (Recall that the ninth parameter, Δt, does not enter into the fit to the non–caustic-crossing data.) Here d is the binary separation in units of the Einstein ring, q is the binary mass ratio, and l is the position along the caustic of the second caustic crossing. For each pair (d, q), one steps along the caustic and determines $A_{\rm cc}$ and u_r from the lens geometry. Equation (5) yields $F_s = (F_{\rm cc} - F_{\rm base})/(A_{\rm cc} - 1)$ and $F_b = F_{\rm base} - F_s$. Next one chooses a value of $t_{\rm E}$. Equation (6) then fixes ϕ: $|\sin \phi| = F_s^2 u_r t_{\rm E}/Q$. This completely determines the geometry and source trajectory (up to a two-fold ambiguity in ϕ).

In practice, Q, $F_{\rm cc}$, and $F_{\rm base}$ all have significant measurement uncertainties, and as Albrow et al. (1999c) discuss, this implies that one must allow a fifth continuous free parameter, ϕ, although this need be considered only over a restricted range. If, as in the present case, light-curve measurements come from several telescopes in several bands, then one must allow additional parameters for the source flux and background flux for each. However, these can be obtained from a simple linear fit (see also below) and so do not add significant computation time. The search through this five-parameter space can be considerably simplified if there is information about the time of first caustic crossing. Then, for each trial trajectory, one can first check if the last measured point before the first caustic indeed lies outside the caustic and if the first point after the first caustic indeed lies inside. If either of these conditions is not satisfied, the trajectory can be rejected without further investigation.

For the second step of the method, we follow Albrow et al. (1999c) with the following exceptions. First, we include the non–caustic-crossing data from all the light curves (except the SAAO V-band data, which are too sparse to contain useful information for this purpose).

Second, we restrict the first caustic crossing to lie between the MPS point before the caustic at HJD′ = 970.0503 and the OGLE point after the caustic at HJD′ = 970.9037. As noted in § 2, the OGLE point could in principle be on the *rising* side of the first caustic crossing, i.e., *before* the center of the source crosses the caustic. However, a MACHO-CTIO R-band data point taken approximately 1.2 hr after the OGLE point rules out this possibility. This point was not reported by Alcock et al. (1999a) because of an oversight but was reported by Rhie et al. (1999). When the relative normalizations of the different light curves are properly set, the MACHO-CTIO point lies 20% ± 10% below the OGLE point. If the OGLE point were before the first caustic, we would expect the light curve to be rising extremely rapidly, by of order a factor of 2 in an hour, just as it is falling very rapidly at the end of the second caustic crossing (Afonso et al. 1998). Thus, the OGLE point certainly occurs on the falling side of the first caustic crossing.

By restricting the first crossing to less than a day, we obtain a much more powerful constraint than the one used by Albrow et al. (1999c), who limited the first caustic crossing only to HJD′ < 973.8. However, this change implies that smaller step sizes are required for $t_{\rm E}$ and sin ϕ so as to avoid missing the first caustic. We choose 2% increments for each, compared to 5% used by Albrow et al. (1999c). Since the two caustics are separated by 12 days, there are guaranteed to be at least three time steps for which the first caustic crossing lies in the designated range.

Finally, to avoid missing rotating wide binaries in the second step, we set the model magnifications equal to unity ($A \equiv 1$) for all points prior to HJD′ = 810 (i.e., about 160 days prior to the first caustic crossing). The MACHO data are fairly flat during this period (Fig. 1). In fact, while many of the binaries that we consider are at baseline during this early period, others, notably wide binaries, are not. They often show a "bump" (brightening then fading) several hundred days before the caustic crossing as the source approaches the companion star. Since this bump is not seen in the data, such binaries would seem to be ruled out. However, it is possible that the companion moved between the time that the source passed closest to the companion and the time when the source crossed the caustic (at which time the geometry of the event was primarily determined). If it moved sufficiently far during this interval, then the source would not have come close enough to the companion to cause a significant bump (see § 6.1). Thus, we include the early data (since it helps set the baseline) but do not allow it to rule out wide binaries until we have had a chance to examine the possibility that they might have avoided detection by rotating.

From this step, we find two allowed regions in (d, q) space. One lies near (d, q) ∼ (0.5, 0.5) and the other near (d, q) ∼ (3.5, 0.4). Albrow et al. (1999a), Alcock et al. (1999a), Udalski et al. (1998b), and Rhie et al. (1999) all considered solutions in the general vicinity of the first region, but none considered solutions near the second. The two allowed regions lie in the lower right and upper left quadrants of the broad range of possible solutions shown in Figure 6 from Albrow et al. (1999c).

For the third step, Albrow et al. (1999c) consider trial trajectories defined by seven parameters: the time $t_{\rm cc}$ and the duration Δt of the caustic crossing, the Einstein timescale $t_{\rm E}$, the projected separation of the binary in units of the Einstein radius d, the binary mass ratio $q = M_2/M_1$, the distance of closest approach (in units of the Einstein radius) of the source to the midpoint of the binary, u_0, and the angle α ($0 \leq \alpha < 2\pi$) between the binary-separation vector (M_2–M_1) and the proper motion of the source relative to the origin of the binary. (The center of the binary is taken to be on the right-hand side of the moving source.) For each observation, the magnification is evaluated in one of two ways. If the source lies at least 3.5 source radii from the caustic, the magnification is simply the magnification of a point source. If it is closer, the finite size of the source is taken into account using the approximation

$$A^{\mathrm{fs}}(\boldsymbol{u}_p) = A_3^0(\boldsymbol{u}_p) + A_2^0(\boldsymbol{u}_q)\left(\frac{\Delta u_{q,\perp}}{\rho_*}\right)^{1/2} G_0\left(-\frac{\Delta u_{p,\perp}}{\rho_*}\right), \quad (8)$$

where $\boldsymbol{u}_p$ is the position in the Einstein ring of the center of the source and $\Delta u_{p,\perp}$ is the perpendicular distances from $\boldsymbol{u}_p$ to the nearest caustic. If $\Delta u_{p,\perp} > \rho_*$, then $\boldsymbol{u}_q = \boldsymbol{u}_p$. Otherwise, $\boldsymbol{u}_q$ is taken to lie along the perpendicular to the caustic through $\boldsymbol{u}_p$ and halfway from the caustic to the limb of the star that is inside the caustic. The perpendicular distance from $\boldsymbol{u}_q$ to the nearest caustic is $\Delta u_{q,\perp}$, $A_3^0(\boldsymbol{u}_p)$ is the magnification of the three nondivergent images at the position $\boldsymbol{u}_p$, $A_2^0(\boldsymbol{u}_q)$ is the magnification of the two divergent images at the position $\boldsymbol{u}_q$, and ρ_* is the source size in units of the Einstein ring. See Figure 3 from Albrow et al. (1999c). The argument of G_0 is negative if the center of the source lies inside the caustic and positive if it lies outside. For each light curve $i = 1, \ldots, 14$, we then use standard linear techniques to find the source flux $F_{s,i}$ and background flux $F_{b,i}$ that minimizes χ_i^2,

$$\chi_i^2 \equiv \sum_k \frac{[F_{s,i} A^{\mathrm{fs}}(t_k) + F_{b,i} - F_k]^2}{\sigma_k^2}, \quad (9)$$

where F_k and σ_k are the measured flux and error for the observation at time t_k. (We follow Albrow et al. 1999c in constraining $F_{s,i}$ to be the same for the five PLANET light curves, $i = 9$, 10, 11, 12, 13 and in constraining $F_{b,10} = F_{b,13}$.)

3.1. *Limb-darkening Parameterization*

Equation (8) is valid in the approximation that there is no limb darkening. We model the surface brightness of the limb-darkened source by

$$S(\theta) = \frac{F_s}{\pi\theta_*^2}\left\{1 - \Gamma\left[1 - \frac{3}{2}\left(1 - \frac{\theta^2}{\theta_*^2}\right)\right]\right\}, \quad (10)$$

where θ is the angular position on the source star relative to its center and Γ is the limb-darkening parameter. Note that with this formulation, there is no net flux in the Γ term, so F_s remains the total flux. Convolving the Γ term with the square root singularity of the caustic, we find the limb-darkened magnification is given by

$$A(\boldsymbol{u}_p) = A^{\mathrm{fs}}(\boldsymbol{u}_p) + \Gamma A^{\mathrm{ld}}(\boldsymbol{u}_p),$$
$$A^{\mathrm{ld}}(\boldsymbol{u}_p) = A_2^0(\boldsymbol{u}_q)\left(\frac{\Delta u_{q,\perp}}{\rho_*}\right)^{1/2} H_{1/2}\left(-\frac{\Delta u_{p,\perp}}{\rho_*}\right), \quad (11)$$

where $H_n(\eta) \equiv G_n(\eta) - G_0(\eta)$ and

$$G_n(\eta) \equiv \pi^{-1/2}\frac{(n+1)!}{(n+1/2)!}\int_{\max(\eta,-1)}^{1} dx \times \frac{(1-x^2)^{n+1/2}}{(x-\eta)^{1/2}}\,\Theta(1-\eta). \quad (12)$$

Explicitly (and correcting a transcription error in Albrow et al. 1999c),

$$G_{1/2}(\eta) = \frac{2}{5}\sum_{\epsilon=\pm 1}(3 + 2\epsilon\eta)(\epsilon - \eta)^{3/2}\Theta(\epsilon - \eta), \quad (13)$$

where Θ is a step function. To allow for limb darkening, we then modify equation (9):

$$\chi_i^2 \equiv \sum_k \frac{[F_{s,i} A^{\mathrm{fs}}(t_k) + F_{\mathrm{ld},i} A^{\mathrm{ld}}(t_k) + F_{b,i} - F_k]^2}{\sigma_k^2}. \quad (14)$$

The limb-darkening parameter for light curve i is then $\Gamma_i = F_{\mathrm{ld},i}/F_{s,i}$.

It is conventional to parameterize limb darkening by

$$S(\theta) = S(0)\left\{1 - c\left[1 - \left(1 - \frac{\theta^2}{\theta_*^2}\right)^{1/2}\right]\right\}. \quad (15)$$

In this case, the flux associated with the limb-darkening term is not zero. Rather, it is a fraction $(3/c - 1)^{-1}$ of the total flux. In a multiparameter problem, the limb-darkening parameter then develops correlations with other parameters with which it has no physical connection. In our formulation, there is no net flux in the limb-darkening term, so the effect of limb darkening rapidly and explicitly vanishes far from the caustic crossing,

$$H_{1/2}(\eta) \to -\frac{3}{160}(-\eta)^{-5/2}, \quad (\eta \ll -1). \quad (16)$$

Thus, there are no spurious correlations. To make contact with the usual formulation, we note that

$$c = \frac{3\Gamma}{\Gamma + 2}. \quad (17)$$

Limb darkening affects the magnification only if the source is transitting or is very close to the caustic. Thus, in principle it could affect the SAAO V and I curves (which both covered most of the caustic crossing), the Yale-CTIO curve (which has one point just before the end of the caustic crossing), the EROS B and R curves (which have 16 points each during the last 110 minutes of the caustic crossing), the MACHO CTIO R curve (which has two points just before the end of the crossing), and the MACHO B and R curves (which have points up to $1.7\Delta t$ *before* the caustic crossing).

While the Yale-CTIO curve does not have enough coverage of the caustic crossing to make an independent estimate of the limb darkening, it is tied to the SAAO photometry as discussed following equation (9) and more thoroughly in § 2 of Albrow et al. (1999c). Thus, this one Yale-CTIO point can enter the fit for the SAAO I limb-darkening parameter. On the other hand, from equation (16) we see that limb darkening affects the MACHO B and R fluxes by less than a fractional amount $\Gamma H_{1/2}(\eta)/G_0(\eta) \sim (3/160)\eta^{-2}\Gamma \lesssim 0.3\%$, where we have assumed $\Gamma \lesssim 0.5$ and where we have made use of the limiting form $G_0(\eta) \sim (-\eta)^{-1/2}$ for $\eta \ll -1$. This compares to typical errors in MACHO photometry for these exposures of 2%–3%. Hence we do not attempt to fit limb-darkening parameters to these two light curves. Thus, we fit for five independent limb-darkening parameters: SAAO V, EROS B, MACHO CTIO R, EROS R, and SAAO I, with corresponding central wavelengths of 0.55, 0.62, 0.64, 0.76, and 0.80 μm.

4. STATIC BINARY SOLUTIONS

We first search for solutions with static binaries. To do so, we will again set $A \equiv 1$ for all points with HJD$' < 810$. In § 6, we will then investigate whether the solutions found in this way (or solutions near them) are in fact permitted when binary rotation is taken into account. We conduct the search on a grid with $(\Delta d, \Delta q) = (0.02, 0.02)$ for the close-binary solution and $(\Delta d, \Delta q) = (0.05, 0.04)$ for the wide-binary solution.

We find two sets of static solutions. One is centered at $(d, q) = (0.54, 0.50)$. At the 3 σ level ($\Delta\chi^2 < 9$), it extends from about $(d, q) = (0.46, 0.42)$ to about $(d, q) = (0.60, 0.58)$ and is about half as wide in the orthogonal direction. The other solution is centered at $(d, q) = (3.25, 0.24)$ and at the 3 σ level extends over the range $d = 3.25^{+0.40}_{-0.20}$ and $q = 0.24^{+0.20}_{-0.16}$. Dominik (1999b) has argued that there is a generic degeneracy in fitting light curves between a pair of close-binary and wide-binary solutions. The second (wide-binary) solution is formally favored at the 2 σ level ($\Delta\chi^2 = 4$), but we do not consider this to be a compelling reason to adopt it as the preferred solution.

All the solutions near the close-binary minimum have similar parameters, as do all the solutions near the wide-binary minimum. For simplicity we quote the full set of parameters only at the minimum. These are shown in Tables 1 and 2. The division between the two tables is such that the parameters shown in Table 2 are derived from the linear fit described by equation (14) and so have associated error bars. The remaining parameters are shown in Table 1. Note that only the first seven parameters in Table 1 are independent. The five remaining parameters are derived from the fit. In particular, $t_* = \Delta t \sin \phi$, and $t_0 = t_{cc} - t_E(u_{cc,x} \cos \alpha + u_{cc,y} \sin \alpha)$. We caution that the numbers of decimal places given for the parameters in Table 1 convey a much higher precision than the statistical errors (which are in fact not even precisely known). The purpose of presenting many decimal places is to allow the reader to reproduce the solution. Because of strong correlations among the parameters, their values in a particular model must be known to high precision in order to avoid misdirecting the model into inappropriate regions of parameter space. The error bars in Table 2 reflect only the correlations within the linear fit described by equation (14) and not the correlations with the parameters in Table 1. Therefore, these are actually lower limits on the errors. Note that we show the ratio F_b/F_s only for the light curves for which it is reasonably well determined ($< 10\%$).

TABLE 1

SOLUTIONS AT THE CLOSE-BINARY AND WIDE-BINARY MINIMA

Parameter	Close Binary (Viable)	Wide Binary (Static) (Not Viable)	Wide Binary (Rotating) (Viable)
d	0.54	3.25	3.65
q	0.50	0.24	0.36
α	350°.575	173°.344	172°.922
u_0	0.045033	0.172928	0.211577
t_E	98.956	164.728	198.323
t_{cc}	982.62408	982.62389	982.62414
Δt	0.17836	0.17889	0.17880
ϕ	36°.9	28°.8	29°.1
t_*	0.1071	0.0862	0.0869
$u_{cc,x}$	0.146824	−1.412225	−1.652962
$u_{cc,y}$	0.021277	−0.009302	−0.007959
t_0	968.63593	751.73636	657.49642
χ^2	981.1	976.8	986.4

The parameter that varies the most over the allowed set of the solutions is t_E, which ranges from about 75 to about 125 days within the 3 σ range of the close-binary solutions and from about 145 to 200 days within the 3 σ range of the wide-binary solutions. From the standpoint of the proper-motion measurement, three parameter combinations are important, $(V-I)_s$, I_s, and $t_* = \Delta t \sin \phi$. The first essentially does not vary at all: $(V-I)_s = 0.30$ for all allowed solutions. When $(V-I)_s$ is fixed, the proper motion scales as $\mu \propto 10^{-0.2 I_s} t_*^{-1}$. The full (3 σ) range of variation of this parameter combination and thus of μ is only about 25% over each the two classes of solutions.

The limb-darkening coefficients given in Table 2 are shown in Figure 2. The close binary is shown by open circles and the wide binary is shown by filled circles. The horizontal error bars show the FWHM of the filters, while the vertical error bars denote the statistical errors. We emphasize again, however, that these include only the errors from the linear fit generated by equation (14) and not those

TABLE 2

SOLUTIONS AT THE MINIMUM DERIVED FROM THE LINEAR FIT OF EQUATION (14)

Parameter	Close Binary (Viable)	Wide Binary (Static) (Not Viable)	Wide Binary (Rotating) (Viable)
Γ (SAAO I)	0.17 ± 0.04	0.15 ± 0.04	0.15 ± 0.04
Γ (EROS R)	0.17 ± 0.04	0.15 ± 0.04	0.15 ± 0.04
Γ (CTIO R)	0.04 ± 0.23	0.01 ± 0.26	0.04 ± 0.25
Γ (EROS B)	0.33 ± 0.04	0.31 ± 0.04	0.31 ± 0.04
Γ (SAAO V)	0.45 ± 0.11	0.41 ± 0.11	0.40 ± 0.11
V_s	22.356 ± 0.007	22.171 ± 0.007	22.527 ± 0.007
I_s	22.058 ± 0.003	21.875 ± 0.003	22.231 ± 0.003
$(V-I)_s$	0.298 ± 0.007	0.297 ± 0.007	0.296 ± 0.007
F_b/F_s (MACHO R)	1.98 ± 0.04	1.51 ± 0.03	2.40 ± 0.04
F_b/F_s (MACHO B)	1.57 ± 0.03	1.16 ± 0.03	1.92 ± 0.03
F_b/F_s (CTIO R)	0.63 ± 0.07	0.65 ± 0.06	1.01 ± 0.08
F_b/F_s (SAAO I)	1.48 ± 0.06	1.14 ± 0.05	1.74 ± 0.07
μ (km s^{-1} kpc^{-1})	1.30 ± 0.08	1.76 ± 0.11	1.48 ± 0.09

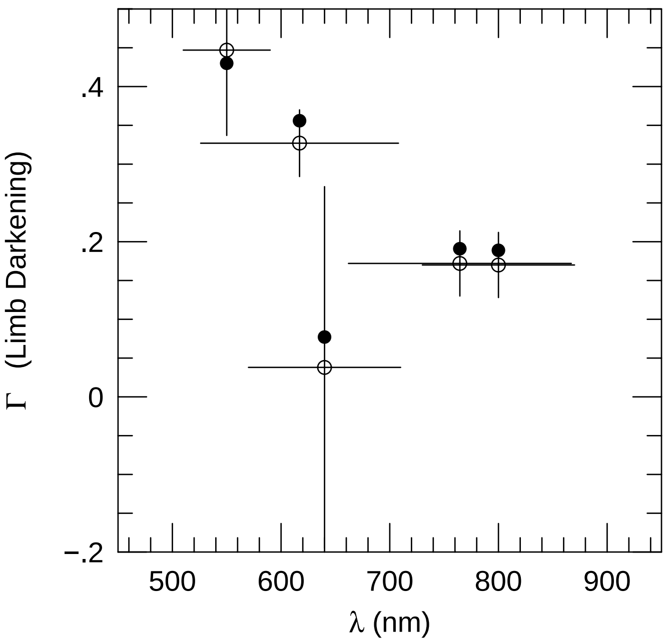

FIG. 2.—Limb-darkening parameters Γ (as defined in eq. [10]) derived from the close-binary solution $(d, q) = (0.54, 0.50)$ (*open circles*) and the wide-binary solution $(d, q) = (3.25, 0.24)$ (*filled circles*) to MACHO 98-SMC-1 for five passbands. *From left to right*: PLANET-SAAO *V*, EROS *B*, MACHO-CTIO *R*, EROS *R*, and PLANET-SAAO *I*. The horizontal error bars represent the FWHM of the filters, and the vertical error bars are statistical. The limb-darkening parameters for the two solutions are very similar because the measurement of limb darkening depends primarily on the caustic crossing and not on the global characteristics of the light curve. To avoid clutter, the error bars for the wide-binary solution are not shown, but they are almost identical to the error bars for the close-binary solution.

that arise from correlations with the other parameters. If we suppress limb darkening and force a fit to a uniform disk, then in both cases χ^2 increases by about $\Delta\chi^2 = 38$ for 5 dof. This is far less than the $\Delta\chi^2 = 106$ that would be predicted based on a naive interpretation of the error bars shown in Figure 2, and this difference arises exactly from the fact that these error bars do not account for the correlations with other parameters. Nevertheless, the full fit reveals that limb darkening has been detected with high significance (formally 99.999%).

Unfortunately, to the best of our knowledge, no theorists have ever calculated limb-darkening profiles of metal-poor A stars. Since limb darkening has clearly been detected in one such star, perhaps some theorist will now undertake such a calculation. For the close-binary solution, the limb-darkening coefficients fall from 0.45 ± 0.11 for *V* to 0.17 ± 0.04 for *I*. The wide-binary solution is similar. The one exception is MACHO-CTIO *R*, but its error bars are too large to make any definite statement because its limb-darkening parameter was derived from only two measurements.

Tables 1 and 2 also show a third solution, one for a *rotating* wide binary. This solution is derived in § 6.1. As is clear from Figure 1, the static wide-binary solution is not viable: it is only an intermediate step on the way to finding a viable rotating wide-binary solution. Hence, in Tables 1 and 2, the close-binary and rotating wide-binary solutions are labeled " viable " while the static wide-binary solution is labeled " not viable." However, until we introduce rotation in § 6, all references to the wide-binary solution will be to the *static* version.

Figures 3 and 4 show the model light curves together with all the available data for the close-binary and wide-binary solutions, respectively. Because the data are in different passbands, we cannot compare the predicted flux with the observed flux as we could if the data were in a single passband. We therefore deblend our data, i.e., we plot $2.5 \log [(F - F_b)/F_s]$ (*points*) and compare this to 2.5 log (magnification) (*solid curve*), where F_s and F_b are the fit values of the source and background flux. The points are binned primarily in 1 day intervals. However, the points before HJD′ = 950 are binned in 10 day intervals and the points near the caustic crossings are binned in 0.1 day intervals. Data from different observatories are combined together. Figures 5 and 6 show close-ups of the two model fits in the neighborhood of the second caustic crossing binned in 0.01 day intervals.

The two fits appear to be equally good to the eye. This is illustrated in Figure 7 which shows the fractional difference in the predicted fluxes between the two models for each of the 14 light curves analyzed in this paper. The fundamental

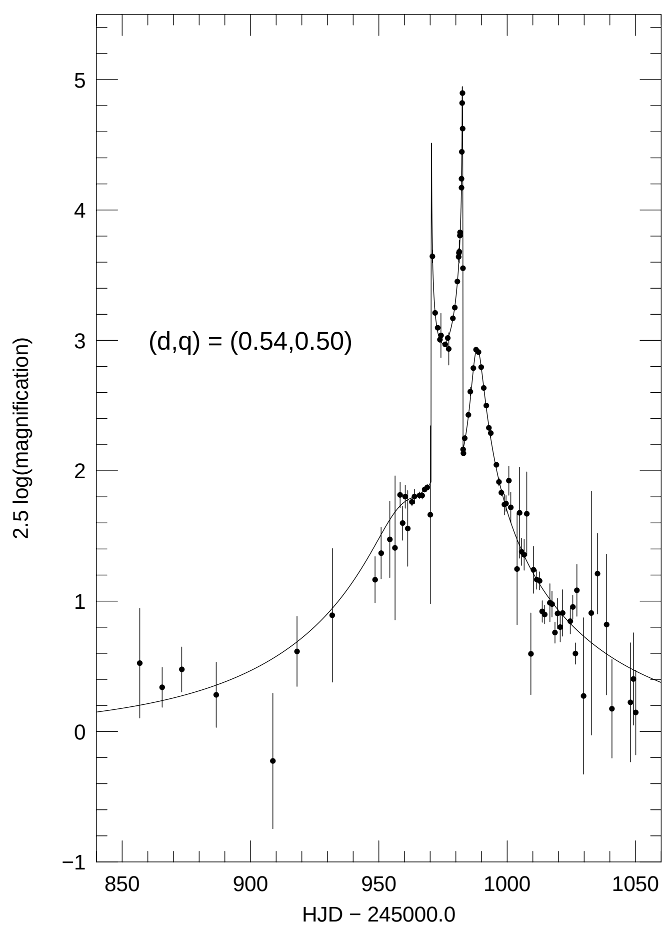

FIG. 3.—Predicted vs. " observed " *deblended* magnification for the close-binary model $(d, q) = (0.54, 0.50)$. The deblended magnification is $A = (F - F_b)/F_s$, where F is the observed flux and F_s and F_b are the fit source and background fluxes in the model. Data are binned, mostly in 1 day bins. However, for HJD′ < 950 there are 10 day bins, and in the immediate neighborhood of the caustics there are 0.1 day bins. Data from all 14 light curves from the five collaborations are averaged together whenever they lie sufficiently close to fit in the same bin.

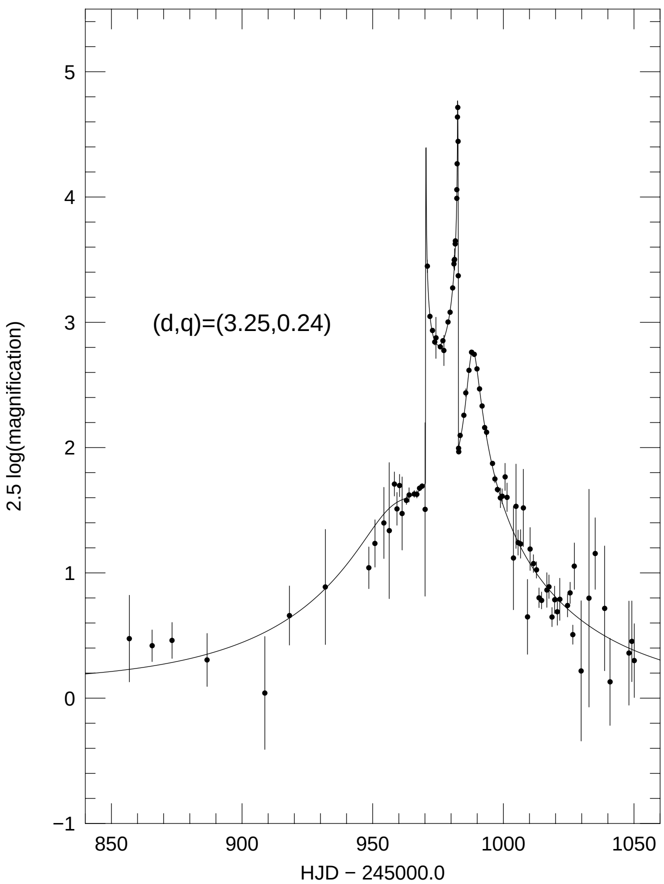

FIG. 4.—Predicted vs. "observed" *deblended* magnification for the wide-binary model $(d, q) = (3.25, 0.24)$. Similar to Fig. 3.

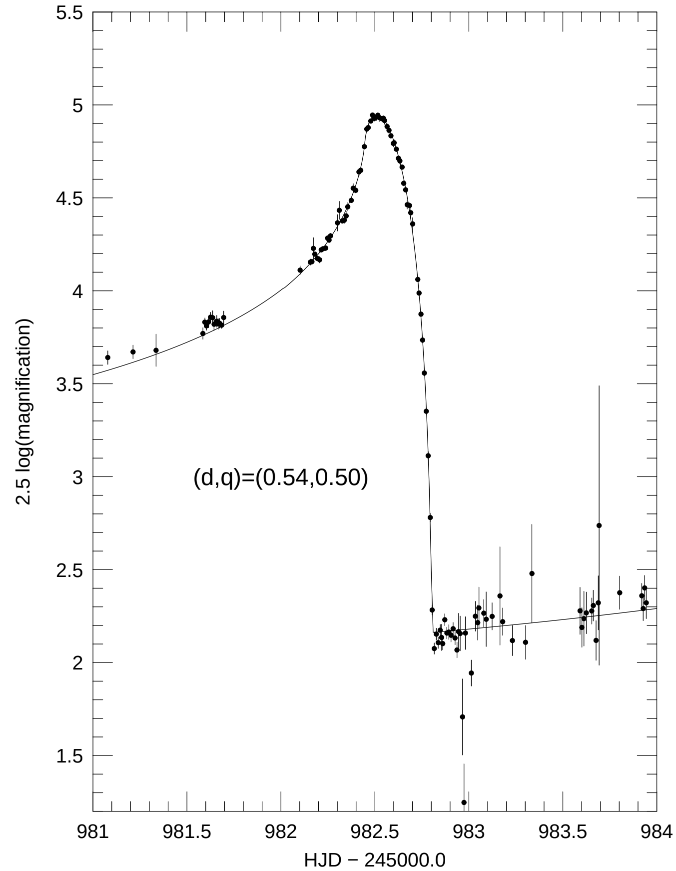

FIG. 5.—Predicted vs. "observed" *deblended* magnification for the close-binary model $(d, q) = (0.54, 0.50)$ showing the vicinity of the second caustic crossing. Same as Fig. 3 except that bins are 0.01 days.

physical reason for this degeneracy is shown in Figure 8, where the caustic structures for the two solutions are superposed. These caustic structures are very similar.

5. PROPER MOTION

The proper motion is given by $\mu = \theta_* / t_*$. To obtain the proper motion one must therefore estimate the angular source size θ_*, which can be calculated if one knows the dereddened color and magnitude of the source. Among all the light curves, there are photometric calibrations for only five: PLANET V (SAAO only) and PLANET I (SAAO and Yale-CTIO) (Albrow et al. 1999a), MACHO B and R (Alcock et al. 1999b), and OGLE I. As we describe below, the calibration of PLANET I is tied to the OGLE calibration. We find that the F_s values for these two light curves are consistent at the 1 σ level. However, the errors for the OGLE I F_s are an order of magnitude larger than for PLANET I (because there are many fewer data points), so the OGLE I F_s does not yield significant additional information about the flux of the source. For the close-binary solution, we have $V_s = 22.36 \pm 0.01$, $I_s = 22.06 \pm 0.00$, and $(V-I)_s = 0.30 \pm 0.01$ from PLANET and $V_s = 22.67 \pm 0.01$, $R_s = 22.58 \pm 0.01$, and $(V-R)_s = 0.09 \pm 0.01$ from MACHO. For the wide-binary solution, we have $V_s = 22.17 \pm 0.01$, $I_s = 21.87 \pm 0.00$, and $(V-I)_s = 0.30 \pm 0.01$ from PLANET and $V_s = 22.48 \pm 0.01$, $R_s = 22.39 \pm 0.01$, and $(V-R)_s = 0.09 \pm 0.01$ from MACHO.

In addition to these errors reported by the fit, Albrow et al. (1999a) estimate that their calibration error is 0.02 mag for the PLANET color and Alcock et al. (1999b) estimate that their calibration error is 0.04 mag for the MACHO color and 0.10 for the magnitudes. Two points are clear from this summary. First, the *ratios* of fluxes are essentially identical for the two models. Second, the MACHO and PLANET colors are mildly inconsistent and the MACHO and PLANET V magnitudes are inconsistent at the 3 σ level. We believe that the PLANET calibration is substantially more reliable than the MACHO calibration since PLANET calibrated their data using secondary standards in the field that were in turn measured in the standard way by OGLE (Udalski et al. 1998a), i.e., from primary standards on photometric nights. On the other hand, although MACHO applies essentially the same procedure for their calibration of their Large Magellanic Cloud (LMC) fields, for the SMC they simply adopt the mean zero points derived for the LMC at similar air mass (Alcock et al. 1999b). We therefore adopt the PLANET calibration.

Following Albrow et al. (1999a), we adopt a total extinction of $A_V = 0.22 \pm 0.1$. The final results do not depend strongly on the extinction (see below). The flux is given by $F = \theta_*^2 S$, where S is the mean surface brightness of the source. We will assume that this surface brightness is a function only of the $(V-I)_0$ color and not any other properties of the star. (We know, for example, that the star is a dwarf rather than a giant.) We can then write

$$\theta_* = 79 \text{ nas} \times 10^{-0.2(I_0 - 22)} \left(\frac{S}{S_{(V-I)_0 = 0.21}} \right)^{-1/2}, \quad (18)$$

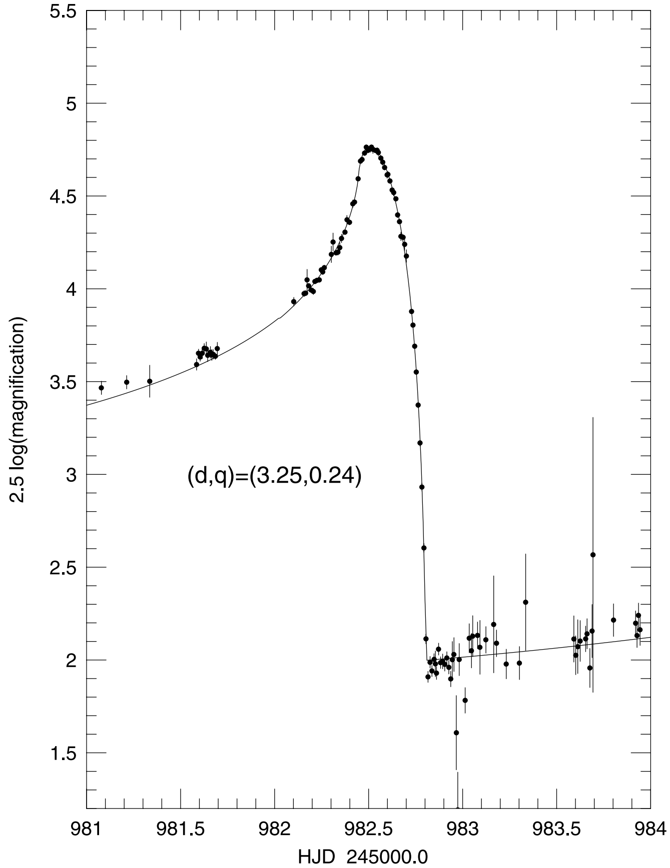

FIG. 6.—Predicted vs. "observed" *deblended* magnification for the wide-binary model $(d, q) = (3.25, 0.24)$ showing the vicinity of the second caustic crossing. Same as Fig. 4 except that bins are 0.01 days.

where we have evaluated the normalization using Green, Demarque, & King (1987), specifically their $Y = 0.2$, $Z = 0.001$, age $= 1$ Gyr table. We therefore obtain estimates of 82 and 89 nas for the angular size of the source in the close-binary and wide-binary solutions, respectively. As described by Albrow et al. (1999a), this estimate has a 3% error for uncertainty in the extinction A_V (Albrow et al. 1999a) and a 5% error for uncertainty in the theoretical model (M. Pinsonneault 1998, private communication), for a total uncertainty of 6%.

Hence, in the two models the proper motions are

$$\mu = 1.30 \pm 0.08 \text{ km s}^{-1} \text{ kpc}^{-1} \quad \text{(close binary)}\,, \quad (19)$$

$$\mu = 1.76 \pm 0.11 \text{ km s}^{-1} \text{ kpc}^{-1} \quad \text{(wide binary)}\,. \quad (20)$$

The errors in these equations reflect only the uncertainties in the extinction and the stellar models, and they do not include uncertainties in the parameter fits. Recall from § 4, however, that even at the 3 σ level, the range of allowed values of the parameter combination $10^{-0.2I} t_*^{-1} \propto \mu$ is very restricted.

The values in equations (19) and (20) clearly put the lens in the SMC rather than the Galactic halo. For comparison, note that Albrow et al. (1999c) found some solutions that were moving much faster and hence would not be explainable as SMC events. These additional solutions are ruled out by combining all the available data.

5.1. *Binary Physical Characteristics*

Since the binary is known to be in the SMC, we can use the proper-motion measurements to obtain estimates of the

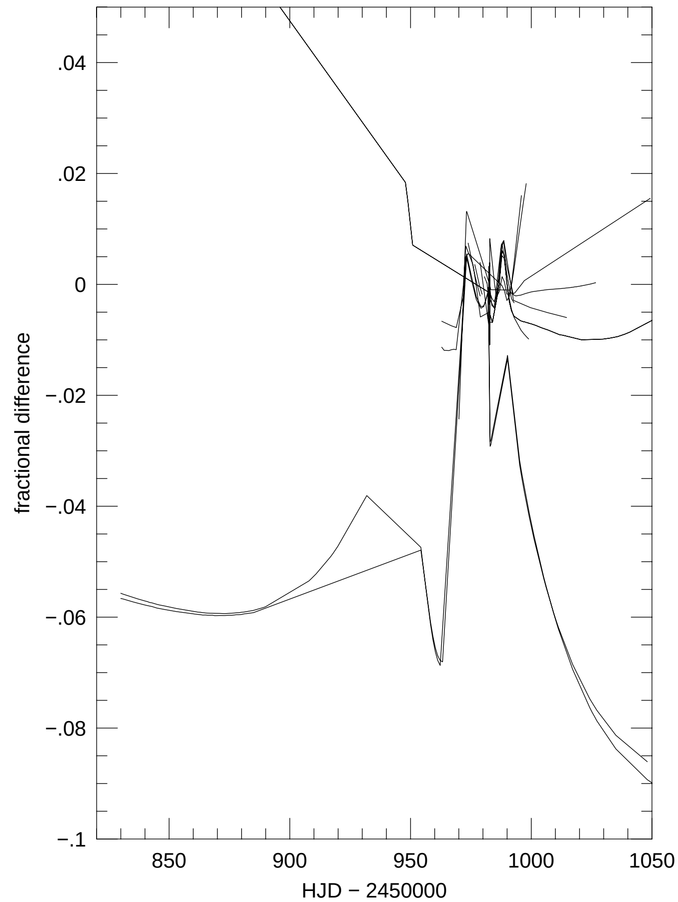

FIG. 7.—Fractional differences between fluxes predicted by the close-binary solution, $(d, q) = (0.54, 0.50)$, and the wide-binary solution, $(d, q) = (3.25, 0.24)$, for the 14 different light curves (*solid lines*).

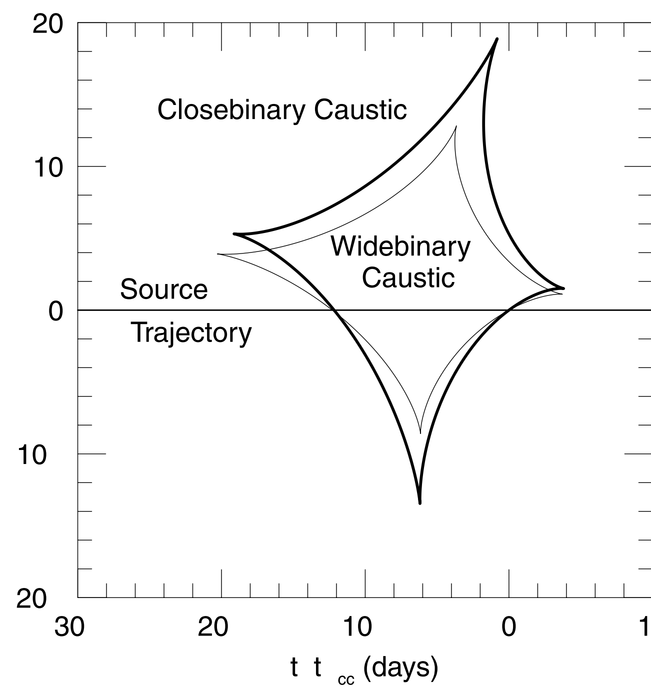

FIG. 8.—Caustic structures for the (*bold curve*) close-binary and (*solid curve*) wide-binary solutions. Each has been rescaled according to the Einstein crossing time of the solution. The caustics have been rotated so that the source trajectories (*straight solid line*) overlap. Time is shown in days from the second caustic crossing, so source motion is to the right.

binary physical projected separation,

$$r_p = d\mu t_E D_S \simeq d\mu t_E \times 60 \text{ kpc} . \tag{21}$$

This yields $r_p = 2.40$ AU and $r_p = 32.4$ AU for the close-binary and wide-binary solutions, respectively. Note that for circular face-on orbits, $r_p = a$, the semimajor axis, while all orbits satisfy $a > r_p/2$.

These projected separations can be used to place limits on the motion of the binary. For example, for the close-binary solution, the blended background flux in the MACHO *B*-band light curve (which has the best determined blended flux and is also the only well-determined measurement in the blue) is approximately 50% larger than the source flux, so the larger of the two lens stars cannot be more than about 2.5 $M_\odot$. For the wide-binary solution, the blended and source fluxes are about equal, so the larger star cannot be more than about 2 $M_\odot$. Thus, the total mass of the binary in both cases is limited to $M \lesssim 3\ M_\odot$. If we momentarily assume a face-on circular orbit, then from Kepler's third law, the period is constrained to $P > 2$ yr and $P > 110$ yr for the two solutions. For a face-on eccentric orbit at apastron, the periods could actually be shorter by $8^{1/2}$, but what actually concerns us is not the length of the period but the relative motion of the binary lenses over times that are very short compared to the period. For a circular orbit, this instantaneous angular speed is $\omega_{\rm circ} = 2\pi/P_{\rm circ}$, but the maximum instantaneous angular speed occurs for a face-on eccentric orbit where the caustic crossing occurs near periastron: $\omega_{\rm max} = 2^{1/2}\omega_{\rm circ}$. We must therefore consider binary motions up to this level.

6. ROTATING BINARIES

Although binaries are not static, only a few attempts have been made to fit microlensing light curves to dynamic binaries (Dominik 1998). In principle, it is possible to measure six orbital parameters of a binary from sufficiently precise observations. These are the same six that can be measured from proper-motion measurements of visual binaries except that the angular semimajor axis is measured relative to θ_E (rather than absolutely) and the line of nodes is measured relative to the direction of the source (rather than celestial coordinates). In practice, it is extremely difficult to measure anything other than the (two-dimensional) projected relative velocity of the components in units of θ_E. In fact, no binary motion information of any type has ever been extracted from a microlensing event. We therefore restrict consideration to the simplest form of such motion, uniform circular motion in the plane of the sky. This leaves the geometry of the lens fixed and permits only rotation of this geometry. If we allowed more general two-dimensional motion, the geometry of the lens would change as the projected positions of the two components moved closer together or farther apart. We will explicitly ignore this type of change in the binary configuration.

6.1. *Wide-Binary Solution*

As we discussed in § 3, we forced the magnification at early times to $A = 1$ when fitting the static binary solutions because the MACHO light curve is observed to be flat at these times. Had we not done so, the wide binary solution would have been ruled out at the 18 σ level ($\Delta\chi^2 = 342$). In Figure 1 we show the early light curve for the best-fit static binary solution together with the MACHO data. The model is clearly ruled out by the data. In fact, we find that even if we allow this binary to rotate with a period of $P = 75$ yr, i.e., the minimum permitted by the argument of § 5.1, the model is still ruled out at the 8 σ level ($\Delta\chi^2 = 58$). However, there are satisfactory rotating binaries in the neighborhood of the best-fit static solution. In Tables 1 and 2 we give the parameters for one of these rotating solutions with $(d, q) = (3.65, 0.36)$ and $P = 75$ yr, and in Figure 9 we show a diagram of the caustic structure for this rotating solution together with the corresponding static solution for the same (d, q). Since the two lenses are separated by much more than an Einstein ring, the magnification structure is for the most part a superposition of the magnification of two isolated lenses. Hence, it is clear from the diagram why the static model is excluded: the source passes within $\sim$0.4 binary mass Einstein radii of the larger lens, which is about 0.55 Einstein radii scaled to the mass of this lens. Thus, the magnification is about 2. Even though the event is heavily blended ($F_b/F_s \sim 2$) and the errors in MACHO photometry

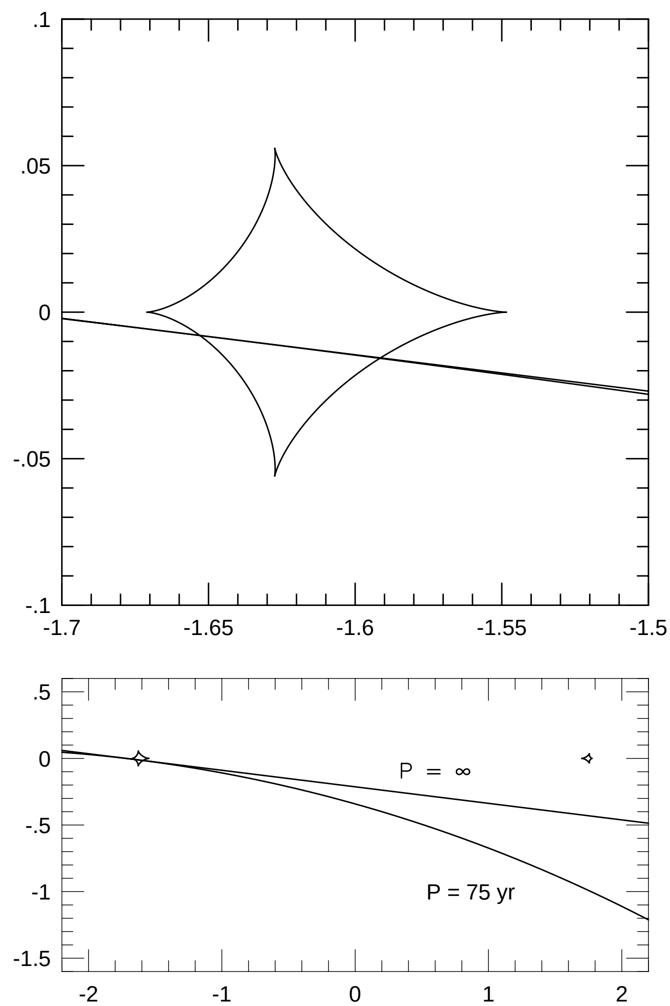

FIG. 9.—Wide-binary trajectory with $(d, q) = (3.65, 0.36)$ for static case and for binary with $P = 75$ yr period. The upper panel shows a close-up of the caustic together with the two source trajectories which are barely distinguishable. The light curve in this region is therefore independent of rotation and the structure of the caustic fixes the local trajectory. The lower panel shows the full caustic structure. The two caustics are separated by about 3.65 Einstein radii, or about 2 yr. This interval is sufficient to allow the source companion closest approach to grow by a factor of $\sim$2 relative to the static case. This in turn reduces $A - 1$ a factor of $\sim$3.5. The static solution is ruled out by the data but the rotating solution is permitted (Fig. 1). The source is moving to the left.

are relatively large at these early times, this magnification would easily be seen in the data. However, if the binary were rotating clockwise in the plane of the sky, then 2 years before the caustic crossing at the time of closest approach, the source would have been about twice as far from the heavier lens, thus reducing $(A - 1)$ by a factor of 3.5. We show the light curve resulting from this rotating binary solution in Figure 1. It is barely distinguishable from the baseline. Numerically we find that the 75 yr period binary increases χ^2 by less than one unit relative to the artificial case used in the initial simulations of $A \equiv 1$ for HJD$' < 810$. We find that the χ^2 of this rotating wide binary is only 5 higher than the χ^2 of the best-fit close binary. We conclude that the data are consistent with a wide-binary solution. The upper panel of Figure 9 is a close-up of the trajectories with and without rotation. The two trajectories are essentially identical in the region around the caustic crossing.

Because the allowed rotating binaries tend to be on one side of best-fit static wide-binary solution (higher d and higher q), they tend to have systematically lower proper motions than that of the static solution given in Tables 1 and 2. For the rotating wide binary shown in Figure 9 (and indeed for its static analog), we find

$$\mu = 1.48 \pm 0.09 \text{ km s}^{-1} \text{ kpc}^{-1} \quad \text{(rotating wide binary)} . \tag{22}$$

6.2. *Close-Binary Solution*

For the close-binary solution the rotation periods can be much shorter, so that in contrast to the situation illustrated in Figure 9 for the wide binary, the rotating and nonrotating trajectories are not the same within the caustic region. Hence, rotating solutions require substantially different geometries. For example, for $P = 10$ yr (counterclockwise), we find a best fit at $(d, q, t_E) =$ (0.56, 0.44, 95.5 days), and for $P = 10$ yr (clockwise), we find $(d, q, t_E) = (0.54, 0.58, 95.9$ days). These solutions are about 1 σ worse fit than the nonrotating solutions. Their proper motions are respectively 4% lower and 7% higher, and the limb-darkening parameters are very similar to the nonrotating case. Thus, while both rotating and nonrotating solutions are compatible with the data and while allowing rotation increases the uncertainties in the binary parameters, these various solutions have very similar implications for the nature of the source and lens.

7. COMPARISON WITH PREVIOUS SOLUTIONS

Six papers have made estimates of some or all of the parameters of MACHO 98-SMC-1 based on subsets of the data presented here (Afonso et al. 1998; Albrow et al. 1999a, 1999c; Alcock et al. 1999a; Udalski et al. 1998b; Rhie et al. 1999). We now analyze the relationship of the results presented in this work to these earlier efforts. We will focus attention on whether the various previous solutions and partial solutions are consistent with one another and with the present results, and we will attempt to resolve any inconsistencies.

Rhie et al. (1999) analyzed almost all of the non-PLANET data presented here, and Albrow et al. (1999c) analyzed almost all of the PLANET data. Hence, our present analysis is essentially based on the union of these two disjoint data sets.

Albrow et al. (1999a) published two solutions, now known as PLANET Model I and PLANET Model II. However, Albrow et al. (1999c) subsequently showed that PLANET Model I actually sits in a *single* extremely broad, virtually flat, χ^2 minimum which connects *all* of the close-binary solutions that they found. PLANET Model I is essentially the same as model 26 from Albrow et al. (1999c). Because of their excellent coverage of the second caustic crossing, Albrow et al. (1999c) were able to measure t_{cc} very precisely and Δt fairly precisely. Those measurements are confirmed by the solutions presented here. On the other hand, they showed that the broad degeneracy in their overall solution could be traced to their lack of coverage of the early light curve (see their Figs. 7, 8, and 9). One would expect as more data are added to the data available to Albrow et al. (1999c) that the two broad minima shown in their Figure 6 would contract and possibly break up into several discrete local minima. The close-binary solution presented here is very similar to an interpolation between the neighboring grid points of their models 27 and 31.

Afonso et al. (1998) measured the parameter combination $t_{cc} + \Delta t = 982.8039 \pm 0.0010$ (after correction of a transcription error in the original paper) based on EROS coverage of the end of the light curve. This differs by only 2 minutes from the values shown in Table 1. Alcock et al. (1999a) modeled the event by combining their own MACHO/GMAN data with the EROS data. The MACHO/GMAN model was refined by Rhie et al. (1999) after the time of the first caustic was pinned down by their own MPS data together with the OGLE data (Udalski et al. 1998b). We now investigate the consistency of the MPS model with the models based solely on the PLANET data on the one hand, and with the close-binary model presented here on the other.

The first question to ask is: are the MPS and close-binary models in discrete local minima, or are they two different points in the same minimum? They are located at $(d, q, t_E) = (0.646, 0.518, 70.5)$ and $(0.54, 0.50, 99.0)$, respectively. To answer this question, we find solutions based on all the data, but subject to the constraint of fixed (d, q). We evaluate these solutions on a grid of $(\Delta d, \Delta q) = (0.02, 0.02)$ in the neighborhood of the close-binary model at $(d, q) =$ (0.54, 0.50). We find that χ^2 varies smoothly over this grid of solutions. The solution at $(d, q) = (0.64, 0.52)$ is extremely similar to the MPS solution, and χ^2 rises monotonically between the close-binary and MPS-like solutions ($\Delta\chi^2 = 32$). Hence these two solutions are in the same minimum and are not discrete minima.

Since the MPS solution has higher χ^2 based on all the data and is in the same minimum as the close-binary solution, did MPS therefore find a false minimum? To address this we evaluate χ^2 for the two solutions based on the data available to MPS (i.e., excluding the PLANET data and the EROS data from other than the night of the caustic crossing and using the SoDoPHOT reductions of the MACHO data rather than image subtraction). We then find that the MPS solution is favored over the close-binary solution by $\Delta\chi^2 = 10$. That is, the two solutions differ because they are based on different data sets rather than because of different modeling procedures.

Finally, we investigate a conflict between the MPS and PLANET solutions which was previously identified by Rhie et al. (1999). They noted that their value of $t_{cc} = 982.683$ or $t_{cc} = 982.694$ (depending on their model of limb darkening) is later than the PLANET value $t_{cc} = 982.62439 \pm 0.00087$ (Albrow et al. 1999c and confirmed here). They did not quote error bars on their own value which is based on modeling the interpolation between MACHO data cutting off 0.3 days before the crossing and EROS data beginning 0.1 days after it. However, by evaluating χ^2 for a series of models with the parameters d, q, α, u_0, t_E, and $t_{cc} + \Delta t$ fixed, but t_{cc} varying, we find that the error in the MPS value for t_{cc} is approximately 0.009 days. Thus, the difference between the MPS and PLANET values is a 6 σ discrepancy if due to an MPS problem and a 68 σ discrepancy if due to a PLANET problem. Clearly this difference is not the product of a statistical fluctuation.

To determine the origin of this conflict, we fit all the data but use the original SoDoPHOT reductions (used by MPS) in place of the image-subtraction reductions (used here) for the MACHO data. We find that the MACHO data points lie systematically above the model at the beginning of night before the caustic crossing (HJD′ $\sim$ 982.1) and systematically below the model at the end of the night (HJD′ $\sim$ 982.3). There is no such systematic trend in the MACHO data points when reduced by image subtraction. We infer that this trend may have been responsible for the late t_{cc} in the MPS model. We test this hypothesis by redoing the fits based on an MPS-like data set but substituting image-subtraction reductions for SoDoPHOT. We then find that the $(d, q) = (0.54, 0.50)$ solution is favored over the $(d, q) = (0.64, 0.52)$ solution by $\Delta\chi^2 = 5$. Moreover, the t_{cc} in the best-fit model now differs from the PLANET value by only 0.02 days, which is only a 2 σ discrepancy.

In brief, the EROS measurement of $t_{cc} + \Delta t$ and the PLANET measurement of t_{cc} have been confirmed with high precision. The original MACHO model when refined by MPS based on the MPS+OGLE determination of the first caustic crossing holds up very well. It lies close to the close-binary solution based on all the data. In hindsight, image subtraction would have yielded even more precise refinements of this model. Finally, one subregion of the broad class of wide-binary solutions found by PLANET (Albrow et al. 1999c) survives the inclusion of the non-PLANET data. We pat our collective selves on the back for a job well done.

8. CONCLUSIONS

We have combined the data on MACHO 98-SMC-1 from five collaborations to produce one of the best sampled microlensing light curves ever published. We confirm earlier claims that the relative source lens proper motion is low, so the lens must be in the SMC. However, there is a twist: despite the fact that our combined data set is enormously superior to any of the individual data sets, there are two very distinct solutions that are compatible with all the data, a close-binary and a wide-binary solution. Fortunately, both have very similar proper motions so there is no significant ambiguity in this parameter. We find a relative proper motion of $\mu \sim 1.30$ km s^{-1} kpc^{-1} or $\mu \sim 1.48$ km s^{-1} kpc^{-1}.

We have measured the limb-darkening parameter in five different bands with centers at 0.80, 0.76, 64, 0.62, and 0.55 μm. If our results are expressed in terms of the standard limb-darkening parameter c, the respective values for the close-binary solution are 0.23 ± 0.05, 0.24 ± 0.05, 0.06 ± 0.34, 0.42 ± 0.05, and 0.55 ± 0.11. All other solutions have limb-darkening parameters that are close to these.

The EROS collaboration wishes to thank J. F. Lecointe for assistance with the online computing, the ESO staff at La Silla Observatory, and the Observatoire de Haute Provence. Work by the MACHO/GMAN collaboration was supported by DOE contract W7405-ENG-48 and DOE grant DEF03-80-ER 40546, NSF grant AST 88-09616, a grant from the Bilateral Science and Technology Program of the Australian Department of Industry, Technology and Regional Development, a PPARC Advanced Fellowship, a Packard Fellowship, and Fondecyt 1990440. Work by the MPS collaboration was supported by a grant from the NASA Origins program (NAG 5-4573), the National Science Foundation (AST 96-19575), by a Research Innovation Award from the Research Corporation, by a grant from the Bilateral Science and Technology Program of the Australian Department of Industry, Technology and Regional Development, and by a grant from the Office of Science and Technology Centers of NSF under cooperative agreement AST 88-09616. Work by the OGLE collaboration was supported by Polish KBN grant 2P03D00814 and NSF grant AST 95-30478. Work by the PLANET collaboration was supported by grants AST 97-27520 and AST 95-30619 from the NSF, by grant NAG 5-7589 from NASA, by grant ASTRON 781.76.018 from the Dutch Foundation for Scientific Research (NWO), and by a Marie Curie Fellowship (grant ERBFMBICT972457) from the European Union. PLANET wishes to thank the observatories that support its science, Canopus, CTIO, Perth, and SAAO, for the large awards of telescope time that make intense microlensing monitoring possible.

REFERENCES

Afonso, C., et al. 1998, A&A, 337, L17
Alard, C. 1999, A&A, preprint (astro-ph/9903111)
Albrow, M., et al. 1999a, ApJ, 512, 672
———. 1999b, ApJ, 522, 1011
———. 1999c, ApJ, 522, 1022
Alcock, C., et al. 1999a, ApJ, 518, 44
———. 1999b, PASP, 111, 1539
Di Stefano, R. 1999, preprint (astro-ph/9901035)
Dominik, M. 1998, A&A, 329, 361
———. 1999a, A&A, 341, 943
———. 1999b, A&A, 349, 108
Green, E. M., Demarque, P., & King, C. R. 1987, The Revised Yale Isochrones and Luminosity Functions (New Haven: Yale Univ. Observatory)
Honma, M. 1999, ApJ, 511, L29
Kerins, E. J., & Evans, N. W. 1999, ApJ, 517, 734
Rhie, S. H., Becker, A. C., Bennett, D. P., Fragile, P. C., Johnson, B. R., King, L. J., Peterson, B. A., & Quinn, J. 1999, ApJ, 522, 1037
Tomaney, A. B., & Crotts, A. P. S. 1996, AJ, 112, 2872
Udalski, A., Szymański, M., Kubiak, M., Pietrzyński, G., Woźniak, P., & Zebruń, K. 1998a, Acta Astron., 48, 147
Udalski, A., Szymański, M., Pietrzyński, G., Kubiak, M., Woźniak, P., & Zebruń, K. 1998b, Acta Astron., 48, 431